Conference on Modelling Fluid Flow (CMFF'22)
The 18th International Conference on Fluid Flow Technologies
Budapest, Hungary, August 30 – September 2, 2022

BUILDING PATTERNS FAVORABLE FOR AIR QUALITY: A PARAMETER STUDY USING LES

Bálint PAPP [1], Gergely KRISTÓF [2]

[1] Corresponding Author. Department of Fluid Mechanics, Faculty of Mechanical Engineering, Budapest University of Technology and Economics. Bertalan Lajos u. 4 – 6, H-1111 Budapest, Hungary. Phone: +36-1-463-2546, E-mail: papp.balint@gpk.bme.hu
[2] Department of Fluid Mechanics, Faculty of Mechanical Engineering, Budapest University of Technology and Economics. E-mail: kristof.gergely@gpk.bme.hu

ABSTRACT

In this paper, a numerical wind tunnel is demonstrated, constructed in a new GPU-based simulation software, in which statistically converged LES results can be obtained within a couple of hours of computational time – a hundred times faster than using conventional CPU-centered CFD models. Using passive turbulence generators near the inlet, the numerical wind tunnel is capable of producing the mean velocity and turbulence intensity profiles characterizing atmospheric boundary layers. In our previous study, the model results were validated with wind tunnel measurements: good agreement was found in terms of both velocity and concentration distributions. The modification of the geometry, as well as the instantaneous flow visualization, is possible during the simulation, enabling the rapid comparison of numerous design concepts.

In the present study, the characteristic velocity and pollutant distributions of typical urban building arrangements – such as street canyons of uniform and heterogeneous roof height, high-rise buildings, as well as vertically elevated buildings with a significant ground clearance – are presented. The optimum building patterns with superior pollutant removal efficiency can be identified by maximizing the mass Stanton number. Based on the parameter studies covering 28 quasi-periodic building patterns of equal volume, recommendations are given for building arrangements to mitigate pedestrian exposure to traffic-induced air pollutants.

Keywords: atmospheric boundary layer (ABL), Computational Fluid Dynamics (CFD), graphics processing unit (GPU), Large Eddy Simulation (LES), pedestrian exposure, traffic-related air pollution

1. INTRODUCTION

Several studies point out the advantages of Large Eddy Simulation (LES) in microscale dispersion modeling via Computational Fluid Dynamics compared to the Reynolds Averaged Navier-Stokes (RANS) approach [1–3]; however, due to its high computational cost, most investigations focus on a single geometry. The analysis of widely varying geometrical parameters using scale-resolving turbulence models is yet to be carried out.

The most frequently investigated parameter of the urban canopy regarding air quality is the street canyons' height-to-width (*H/W*). However, Da Silva et al. [4] concludes that this aspect ratio in itself is not enough to assess street ventilation, even for uniform building height; and other parameters, such as the porosity of the canopy and the size and placement of openings to the wind, can influence the concentration distribution substantially.

Apart from the uniform street canyon geometry, several studies provide information on more complex building configurations, such as asymmetric street canyons [5], lifted up buildings (with significant ground clearance) [6], and arrays consisting of high-rise buildings of uniform and variable height [7–9].

Recommendations for favorable building shapes are compiled in the recent review paper by Huang et al. [10]; moreover, the impact of several geometrical parameters on pollutant transport is summarized by Kluková et al. [11], both highlighting the favorable effect of building height non-uniformity. A comprehensive literature survey was also carried out by Palusci et al. [12] on the impact of the above-mentioned and additional morphological parameters on urban air quality, such as the roof shape, the plan area density and the frontal area density.

In the present study, the total building volume of the investigated building layouts and the installation raster size – which are important economic and urban planning parameters – are set at constant values, following the approach of Kristóf and Füle [13].

2. METHODOLOGY

In this paper, a numerical wind tunnel (Figure 1) is utilized, based on a real boundary layer wind tunnel of the Institute for Hydromechanics of Karlsruhe Institute for Technology (KIT), which was previously validated [14] and applied for urban dispersion studies [15, 16]. Note that the GPU-based LES model was also found applicable for testing the dynamic wind loads of buildings [17, 18].

The numerical wind tunnel, identically to the original, has a model scale of M = 1:150, and it consists of a 19H long flow preparation section (fetch) and an 11H long test section. The width and height of the numerical wind tunnel are 16H and 5H. The reference length is H = 120 [mm] (thus 18 [m] in full scale), which is equal to the uniform building height of simple H/W = 1 aspect ratio street canyons.

2.1. Building Patterns

The main goal of the present study is to analyze and compare several periodic building patterns (examples are shown in Figure 2) in order to find the optimum geometrical arrangement of a given building volume for the best air quality; hence, the total volume of the building configurations presented in this paper is kept constant.

As a reference case, a series of **uniform street canyons** were investigated. Using six rows of buildings, five H/W = 1 aspect ratio street canyons were constructed perpendicular to the wind direction in the test section of the numerical wind tunnel, containing a $W/2$ wide emission zone at the bottom of the canyons representing the traffic lanes. The laterally oriented street canyons are divided by two streamwise cross streets into two 2H wide section at

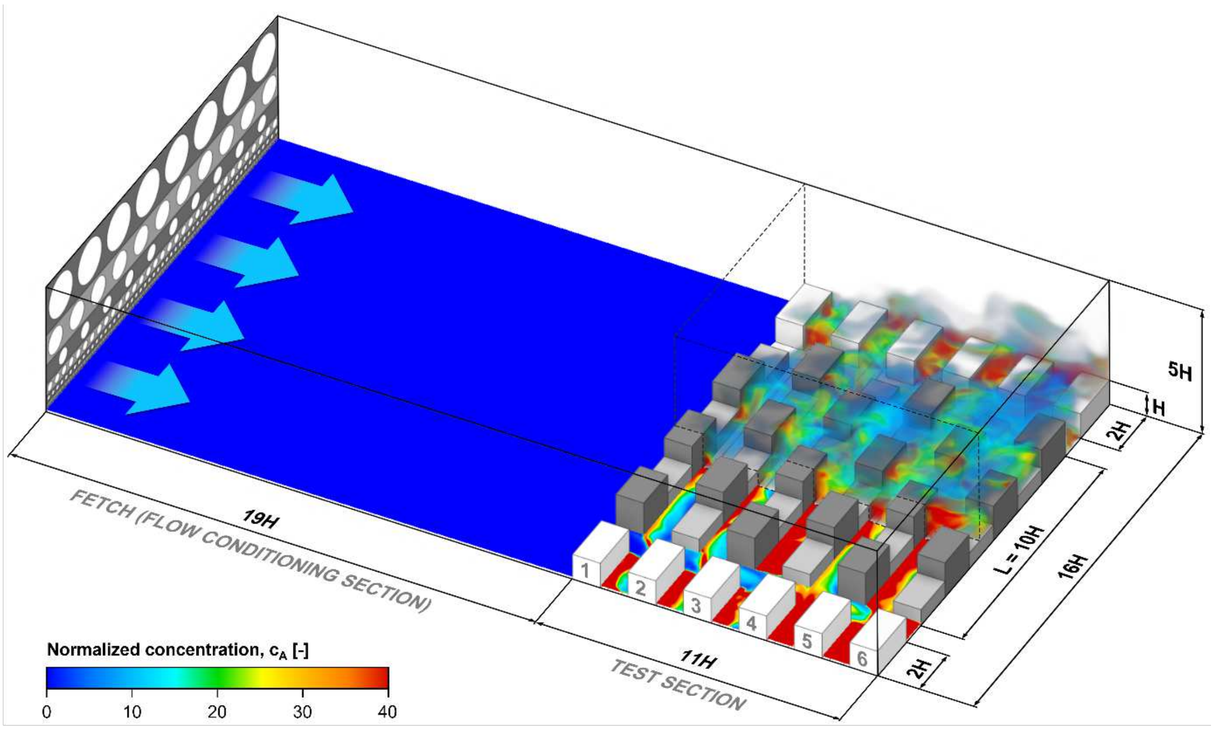

Figure 1. Layout and dimensions of the computational domain relative to the reference building height H = 120 [mm]. The horizontal cut plane shows the instantaneous normalized concentration distribution at pedestrian head height (z/H = 0.0833) for a staggered tower arrangement. Within the volume designated by dashed lines, the 3D dispersion field is displayed.

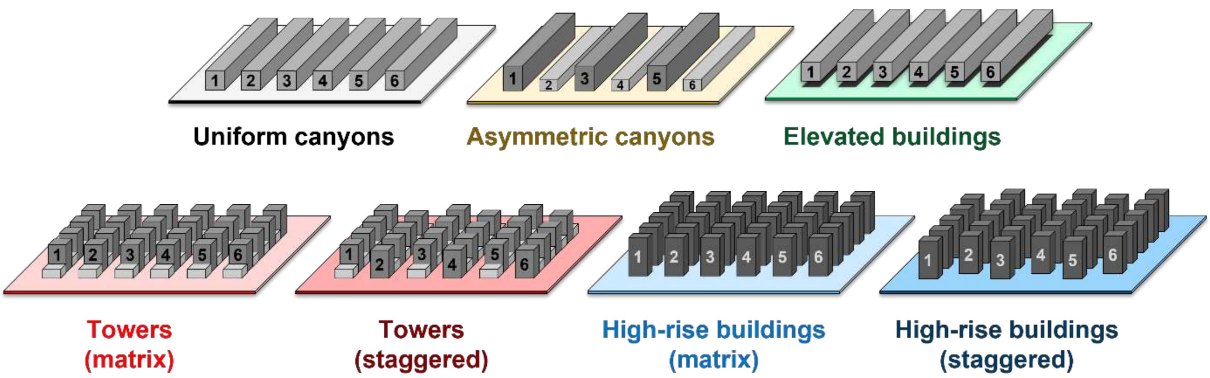

Figure 2. Schematics of the investigated building patterns. Wind direction: from left to right.

the sides and one $L = 10H$ wide section in the middle, as shown in Figure 1. The present investigation focuses on the $L = 10H$ wide central section only.

Asymmetric street canyons can be constructed from the uniform canyons by increasing and decreasing the roof height of consecutive buildings by $\pm\Delta z$. Therefore, each building has a constant roof height along the lateral direction ($H+\Delta z$ or $H-\Delta z$), i.e., the roof height varies only in the streamwise direction, and it is homogeneous in the lateral direction. In these cases, the impact of the roof height heterogeneity ($\Delta z/H$) will be investigated (see Section 3.1 for the results). Note that two simulations were run for each roof height offset: in one, even-numbered buildings were taller, while in the other, the odd-numbered ones. The reason for this is that the flow and dispersion fields are significantly different in the case of finite rows of buildings starting with a short building compared to starting with a tall one. The results for these two arrangements were later averaged to obtain the final ventilation indices.

Towers can be constructed on top of the buildings by dividing the blocks within the $L = 10H$ wide central section laterally and changing the roof height by $\pm\Delta z/H$ of each segment. The width of the towers is $T = L/2N$, in which N is the tower count in a single row ($N = 2, 3, 4, 5$ in this paper). Towers can be placed in the so-called **matrix (aligned) arrangement**, in which there is a full overlap in the streamwise direction between the towers in consecutive streets ($\Delta y/T = 1$), resulting in the roof height varying in the lateral direction only. On the other hand, in the so-called **staggered arrangement**, towers are followed by shorter building sections in the streamwise direction (and vice versa, thus $\Delta y/T = 0$), so the roof height varies in both streamwise and lateral directions (see also Figure 1). For the two tower configurations, the impact of the tower width (T/H, analogous to the impact of the tower count N; see Section 3.2 for the results), and the impact of the tower height ($\Delta z/H$; see Section 3.3) will be analyzed for both matrix and staggered arrangements.

If the roof height offset of the towers is $\Delta z/H = 1$, the resultant geometry consists of fully separated **high-rise buildings**, each of $2H$ height. In these cases, the approach flow can directly access the emission zones at ground level, which is unprecedented in any of the above-mentioned configurations. For these types of building patterns, the impact of the streamwise overlap of the buildings between consecutive rows ($\Delta y/H$) will be studied for both $N = 3$ and 5 towers in a single row (Section 3.4).

Finally, the **uniform buildings** of the reference case can be **vertically elevated**, which also enables the direct transport of pollutants away from the source zones, similar to the high-rise buildings. The impact of the ground clearance (i.e., the gap between the ground and the buildings, $\Delta z/H$) will be investigated (Section 3.5).

2.2. Simulation Setup

For CFD modeling, the GPU-based simulation software ANSYS Discovery Live 2019R3 was used, which was originally developed for mechanical engineering optimization applications. During the transient flow simulations coupled with heat transfer, the continuity, Navier-Stokes and energy equations are solved using the Finite Volume Method (FVM) for discretization. Turbulence is modeled using the standard Smagorinsky subgrid-scale stress model [19] with $C_s = 0.1$.

For resolving the geometries, an equidistant Cartesian mesh is applied, the cell count of which is dependent on the VRAM capacity of the utilized GPU. In the present study, an Nvidia GTX 1080Ti graphics card was employed with 11 GB VRAM, resulting in a total of 9.1 million cells in total. The $H/W = 1$ aspect ratio of the street canyon was chosen as a sweet spot between the number of street canyons and the spatial resolution of each canyon: this way, we have the opportunity to observe five street canyons with the building height and the street width both being resolved by 16 cells, which is sufficiently high for capturing the large-scale eddies governing the dispersion processes using LES [20]. The time step size is adaptively set during the simulation based on the Courant-Friedrichs-Lewy condition [21], with the maximum of the Courant number being kept around $C_{max} = 1.8$, resulting in an average time step size of $5.2\cdot10^{-4}$ [s]. Note that a single simulation case required only a couple of hours to cover 20 [s] of physical time (in $M = 1{:}150$ model scale), the last 15 [s] of which was used for time-averaging.

The simulation details and the solution methods of the applied software are given in [18]**.** Note that the latest release at the time of publishing, ANSYS Discovery 2022R1, is capable of performing a fully unstructured FVM similar to the general unstructured FVM in ANSYS Fluent but implemented for GPU HPC.

Atmospheric dispersion processes – both in wind tunnels and in numerical modeling – are notoriously sensitive to the characteristics of the approach flow, i.e., the proper specification of the atmospheric boundary layer (ABL), which in our case is characterized by the below mean velocity and turbulence intensity profiles.

$$u(z) = u_H \cdot (z/H)^{\alpha_u} \tag{1}$$

$$I_u(z) = I_{u,H} \cdot (z/H)^{\alpha_{I,u}} \tag{2}$$

In the above formulas, u [m/s] denotes the streamwise mean velocity, I_u [%] is the turbulence intensity, and z [m] is the vertical coordinate. Moreover, $u_H = 4.64$ [m/s] and $I_{u,H} = 20.98$ [%] are the reference velocity and reference turbulence intensity values taken at roof height $H = 120$ [mm], and $\alpha_u = 0.30$ [–] and $\alpha_{I,u} = -0.36$ [–] are the profile exponents. The characteristic Reynolds number

$Re_H = u_H H/\nu = 37{,}000$ is sufficiently high to assume that the flow and dispersion fields are independent of the Reynolds number [22, 23].

In the present study, an unconventional inlet design (shown in Figure 1 and described in detail in [14]) is employed in order to shorten the length of the flow preparation section. The resultant streamwise mean velocity and turbulence intensity profiles at the beginning of the test section (19*H* downstream from the inlet) showed good agreement with the wind tunnel profiles (described by coefficients of determination $R^2 = 0.982$ and 0.927), as displayed in Figure 3 below.

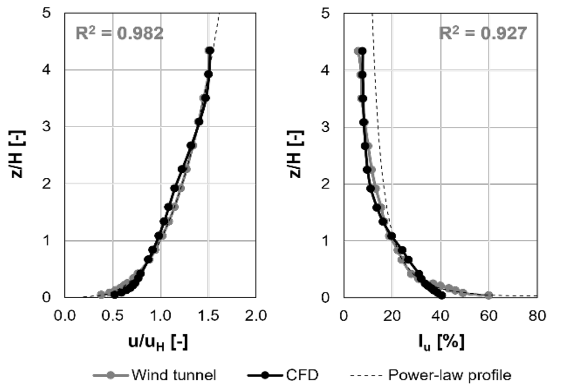

Figure 3. Approach flow profiles: normalized mean velocity and turbulence intensity.

The simulation domain is bounded by symmetry boundary conditions at the lateral sides and at the top. At the solid surfaces, the no-slip condition is maintained. At the downstream boundary 0 [Pa] gauge pressure is assumed.

2.3. Dispersion Modelling Using a Thermal Analogy

In order to simulate the dispersion of traffic-induced air pollutants, a thermal analogy must be applied [14], necessitated by the fact that ANSYS Discovery Live 2019R3 cannot handle user defined scalars (nor can the latest release, ANSYS Discovery 2022R1). The analogy is based on the identical forms of the diffusive and the thermal transport equations of constant property fluids (shown below), supplemented with identical boundary conditions.

$$\frac{dc}{dt} = \nabla \cdot (D\nabla c) \tag{3}$$

$$\frac{dT}{dt} = \nabla \cdot (a\nabla T) \tag{4}$$

In the above equations, c [kg/m^3] denotes the concentration of non-settling, passive pollutants in the air, t [s] is time, T [K] is the absolute temperature, while D and a are the diffusivity and thermal diffusivity coefficients expressed in the same kinematic unit [m^2/s]. The thermal analogy requires the heat conductivity of the fluid to be chosen for the Lewis number to be one ($Le = a/D = 1$); thus, the heat conductivity of air λ [W/(m·K)] in the numerical model is set to

$$\lambda = D\rho c_p \, , \tag{5}$$

where ρ [kg/m^3] is the density, and c_p [J/(kg·K)] is the specific heat of air. Note that in the energy balance both the expansion work and the viscous dissipation need to be neglected.

In conclusion, in the thermal analogy, the temperature field represents the spatial distribution of air pollutants (with 0°C indicating clear air), and the vehicle emissions are taken into account by temporally constant heat sources placed at the traffic areas.

2.4. Ventilation Indices

In the present paper, air quality and the ventilation effectiveness of the different building configurations are assessed using three main properties.

The **normalized velocity** is calculated as

$$u/u_{BL} \, , \tag{6}$$

in which u [m/s] is the streamwise mean velocity and u_{BL} [m/s] is the freestream velocity, i.e., the streamwise mean velocity obtained by spatially averaging at the top of the domain. This approach guarantees that the artificial acceleration of the flow over the urban canopy – caused by the limited domain height and the moderate blockage ratio (20…40%) – are taken into account in the results.

Building patterns of higher roughness, that is, the ones with more heterogeneity in building height, extract more energy from the atmospheric boundary layer. Therefore, some previous investigations employ the friction velocity $u^* = (\tau/\rho)^{0.5}$ for normalization to account for the deceleration of the wind [13]. In contrast to this long-term approach, the present analysis focuses on the local effects, which is also a reasonable and widely used alternative in experimental and computational dispersion studies.

To assess the exposure of pedestrians and residents to traffic-related air pollution, the **normalized concentration** is defined as

$$c_A = \left[\frac{u_{BL}T \cdot \rho c_p}{Q_{heat}/A}\right]_{model} = \left[\frac{u_{BL}c}{Q_{poll}/A}\right]_{real} , \tag{6}$$

in which A [m^2] is the total plan area of the investigated region and Q_{heat} [W] is the source intensity, i.e., the amount of heat introduced to the system through the aforementioned area. Note that if the freestream velocity, the total plan area of a real location and the corresponding pollutant emission intensity Q_{poll} [kg/s] is known, the real pollutant concentration distribution c [kg/m^3] can be realized based on the model results.

Finally, the **mass Stanton number**, i.e., the dimensionless mass transfer coefficient or dilution coefficient, corresponding to the ventilation efficiency of each building pattern, can be calculated as the reciprocal of the normalized concentration:

$$k_A = \frac{1}{\langle c_A \rangle} \quad (7)$$

Note that the average normalized concentration $\langle c_A \rangle$ in the above formula can be calculated following two slightly different approaches:

1) based on the average concentration **at pedestrian head height** (at z/H = 0.0833 for the present buildings) corresponding to the pedestrian exposure to traffic-related air pollutants, or
2) based on the average concentration **below roof height** ($z < H_{max} = H + \Delta z$) corresponding to the exposure of the residents of the buildings.

3. RESULTS AND DISCUSSION

In the following sections, the impact of five different geometrical parameters will be analyzed. The discussion of the results mainly focuses on the near-ground normalized concentration as the canopy average concentration significantly decreases in all cases compared to the reference case. The detailed numerical quantitative results for all 28 simulation cases can be found in Table A1 in the Appendix.

3.1. The Impact of the Roof Height Heterogeneity in Asymmetric Street Canyons

According to Oke [24], a so-called skimming flow regime develops over densely packed buildings similar to the majority of the building configurations presented in this study. In the case of a series of parallel, H/W = 1 aspect ratio street canyons for perpendicular wind direction, the flow field below roof height is principally governed by the canyon vortex (with a horizontal axis of rotation) at the middle of the 10H long buildings and the vertically rotating corner eddies forming near the intersections (see Figures A1 and A2 in the Appendix).

In asymmetric canyons, the street is bordered by $H \pm \Delta z$ tall buildings, and a more complex vortex structure is formed. The results shown in Figure 4 indicate that smaller (although still substantial) roof height offsets ($\Delta z/H$ = 0.25 and 0.375) cannot mitigate the pedestrian exposure. However, for greater offsets ($\Delta z/H$ = 0.5 and 0.75) resulting in particularly asymmetric street canyons (H_{max}/H_{min} = 3 and 7), the effective aspect ratio of the street canyons formed by every second building increases; hence, the resultant velocity field resembles the wake interference flow regime described by Oke [24]. In these configurations, the large horizontal vortices located between the tall buildings (and above the short ones) become more dominant, and they can effectively transport the traffic-induced air pollutants above roof level, resulting in a concentration decrease of 32% at pedestrian head height.

3.2. The Impact of the Tower Width and Tower Count

A series of simulations with different tower counts were performed with a $\Delta z/H$ = 0.375 roof height offset, resulting in a ratio of the building heights of H_{max}/H_{min} = 2.2. Note that this offset was not able to improve the near-ground air quality for asymmetric street canyons (see the previous section).

It is shown in the upper part of Figure 5 that towers in **matrix (aligned) arrangement** are also unable to improve the near-ground air quality, regardless of the tower count. On the other hand, the air quality of the entire canopy improves by over 30%: the decrease of the average concentration below roof height is the consequence of the wind penetrating the canopy between the towers and letting the pollutants escape from the upper region more efficiently.

In the case of the **staggered tower arrangement**, however, the tower count does matter, as the increased mixing between the towers (illustrated in Figure A2/d in the Appendix) is capable of facilitating an increased wind speed at

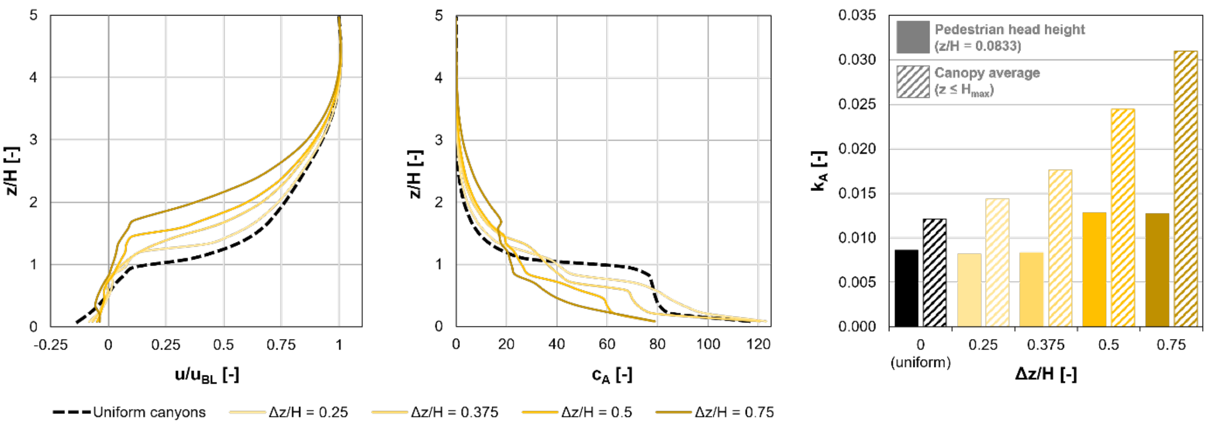

Figure 4. Asymmetric canyons: the impact of the roof height offset ($\pm\Delta z$), compared to the uniform canyons reference case ($\Delta z = 0$). The height difference between the short and tall buildings is actually $2{\cdot}\Delta z$. The figure shows the vertical profiles of normalized velocity and concentration as well as the ventilation efficiency.

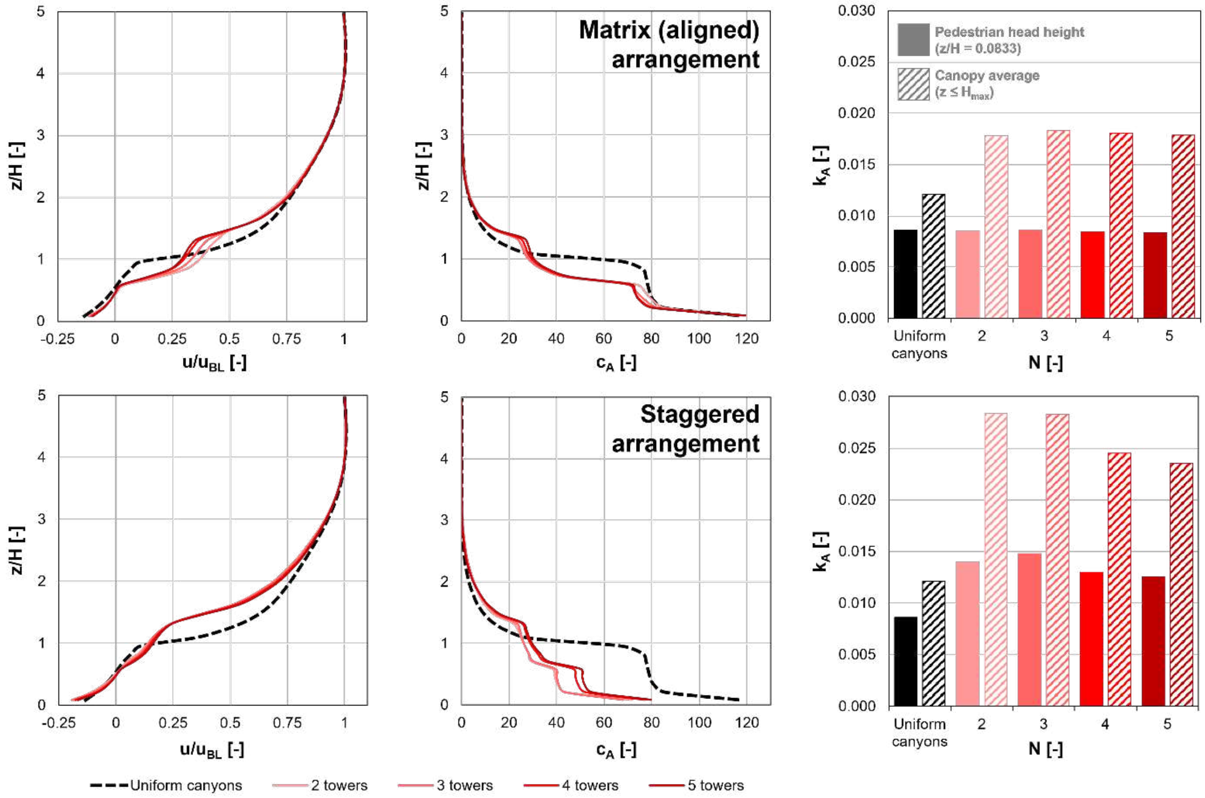

Figure 5. Towers: the impact of the tower count in a single row (*N*), compared to the uniform canyons reference case. The roof height offset is $\Delta z/H$ = 0.375 for all non-reference cases. The figure shows the vertical profiles of normalized velocity and concentration as well as the ventilation efficiency.

ground level; thus, more efficient pollutant removal is achieved from pedestrian head height. It can be seen in the lower part of Figure 5 that the near ground concentration can be decreased by 38…42% for 2 and 3 towers, while in the presence of 4 and 5 towers, the air quality can be improved by 31…34% compared to the reference case consisting of a series of uniform street canyons. The most favorable three-tower case has a tower width of $T = L/6 = 1.667H$.

3.3. The Impact of the Tower Height

In order to figure out how the air quality depends on the tower height, the superior three-tower setup was further investigated for both the matrix and the staggered arrangement.

Based on the results shown in Figure 6, high rise buildings (corresponding to $\Delta z/H = 1$) should be clearly separated from the rest of the cases in the **matrix (aligned) arrangement**; as the wind can directly reach the emission zones to sweep away the near-ground pollutants, resulting in a significant decrease of the pedestrian exposure (–42%). In contrast to this configuration, towers placed on top of the base buildings in the matrix arrangement are not able to improve the air quality in the near-ground region, regardless of the tower height.

In contrast, for the **staggered arrangement of** the towers, the pedestrian exposure gradually decreases with the tower height (–32…45% in pedestrian head height); moreover, staggered high-rise buildings (in this case, three in each row) can mitigate the pedestrian exposure to traffic-induced air pollutants by 46%.

3.4. The Impact of the Streamwise Overlap of the High-Rise Buildings

Let us now analyze the effect of the streamwise overlap of the high-rise buildings of the consecutive rows (relative to the tower width: $\Delta y/T$) on air quality in the case of both three and five buildings per row.

It is reinforced by the results shown in Figure 7 that fewer but broader buildings are more favorable for air quality, at least in the first few rows directly subjected to the approach flow, most likely because the wind can penetrate the canopy deeper due to the wider gaps between the buildings.

Shifting the high-rise buildings laterally, starting from the matrix arrangement (full overlap, $\Delta y/T = 1$) causes more surface to obstruct the wind, which is hence slowed down to a higher degree below roof height, although the mixing is enhanced (see Figure A3 in the Appendix). Depending on the building overlap, however, the mean near-ground concentration decrease is between 42% and 55% for three towers, and between 25% and 32% for five towers, thus the matrix ($\Delta y/T = 1$), intermediate ($\Delta y/T = 0.5$) or staggered ($\Delta y/T = 0$) high-rise buildings are all remarkably efficient solutions for locally mitigating exposure to traffic-related air pollutants compared to a series of uniform street canyons.

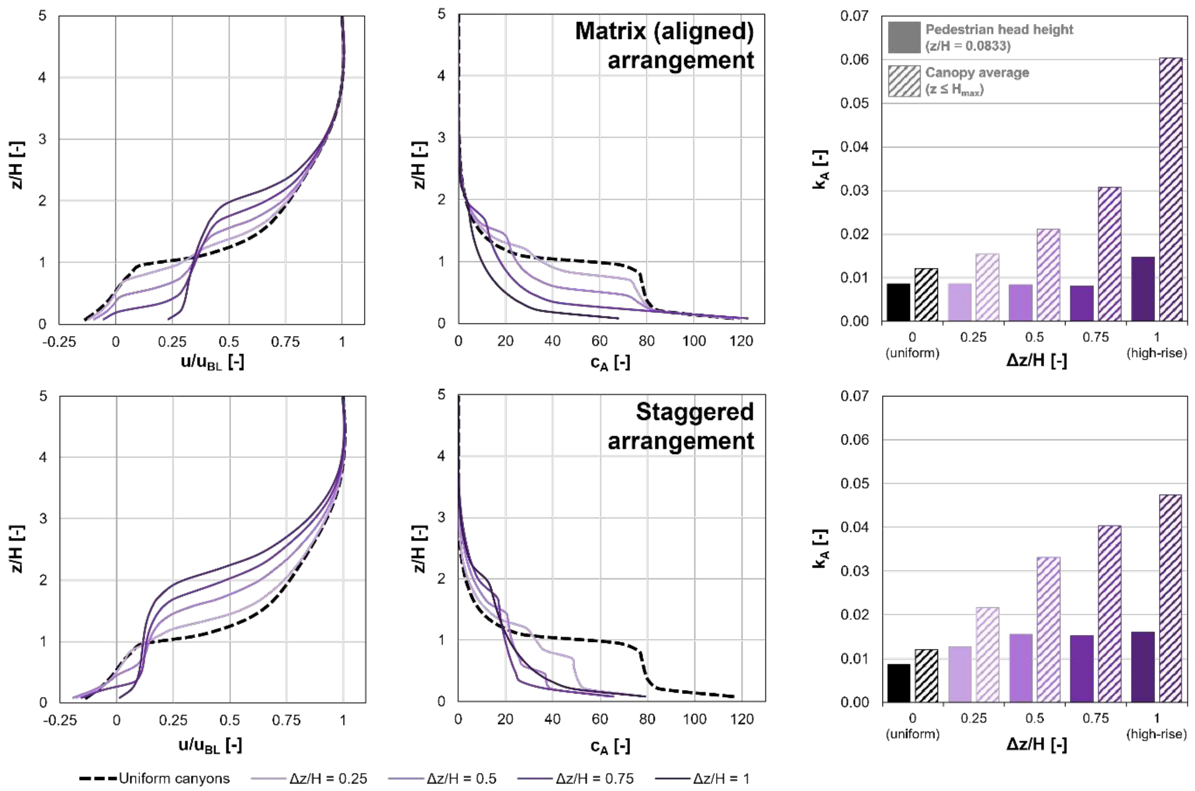

Figure 6. Towers: the impact of the tower height offset ($\pm\Delta z$), compared to the uniform canyons reference case. The height difference between the short and tall buildings is actually $2\cdot\Delta z$. The tower count is $N = 3$ for all non-reference cases. Note that $\Delta z/H = 1$ corresponds to high-rise buildings. The figure shows the vertical profiles of normalized velocity and concentration as well as the ventilation efficiency.

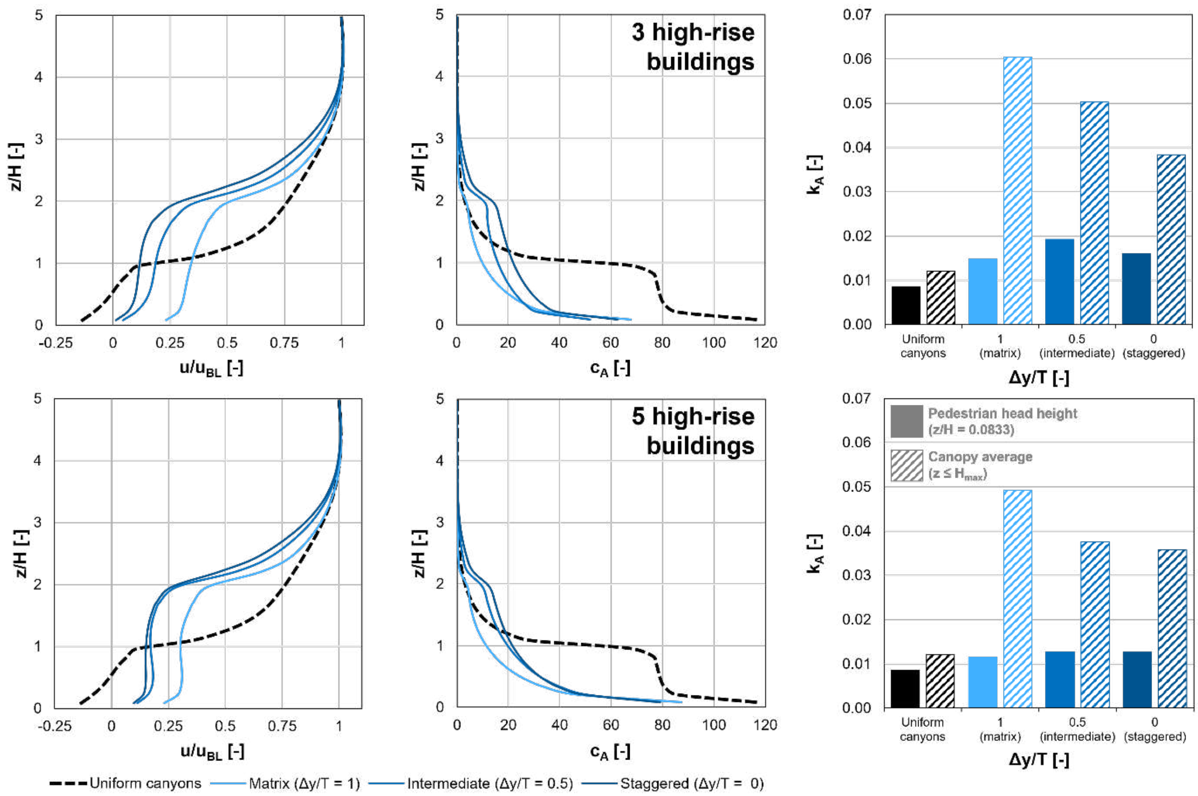

Figure 7. High-rise buildings: the impact of the streamwise overlap of the buildings in consecutive rows (Δy), compared to the uniform canyons reference case. The building height is $2H$ in all non-reference cases. The figure shows the vertical profiles of normalized velocity and concentration as well as the ventilation efficiency.

3.5. The Impact of the Building Elevation

Direct access to the pollutant emission zones can also be achieved by elevating the buildings forming the uniform canyons vertically, that is, by creating a gap at the location of the ground floor.

It is shown in Figure 8 that a ground clearance of $\Delta z/H = 0.1667$ (corresponding to 3 [m] in full scale) is already able to reduce the near-ground concentration by 29%, and if the ground clearance is increased to $\Delta z/H = 0.3333$, the concentration decrease is 60% based on the results of the first five canyons of the city.

Basal openings can cause excessively high near-ground velocities, which is disadvantageous for pedestrian wind comfort. Moreover, as shown in Figures A1 and A2, a stark streamwise near-ground concentration gradient is present as the wind speed decreases and the pollutants accumulate due to the hydraulic resistance of the urban canopy. This implies that the elevation of the buildings could be effective only in the first few canyons that are subjected directly to the wind (e.g., located on the border of the city or next to a larger opening inside).

4. CONCLUSIONS AND OUTLOOK

In this paper, the ventilation characteristics of 28 different periodic building arrangements of equal total volume were analyzed using GPU-based Large Eddy Simulation in ANSYS Discovery Live 2019R3. The pedestrian exposure to traffic-induced air pollutants was characterized by the normalized near-ground pollutant concentration as well as the mass Stanton number, i.e., the dimensionless mass transfer coefficient of the building configurations.

The most important findings are listed below, based on the comparison to a baseline case consisting of a series of $H/W = 1$ aspect ratio parallel street canyons subjected to a perpendicular atmospheric boundary layer approach flow. The results cover six consecutive rows of buildings (thus five streets), and it is acknowledged that the results can differ in the longer run.

a) Asymmetric street canyons are only able to mitigate the pedestrian exposure if the effective street canyon aspect ratio is high enough, i.e., if every second building is rather short ($\Delta z/H > 0.5$).
b) For towers placed on top of shorter continuous buildings in matrix (aligned) arrangement, the near-ground concentration cannot be improved regardless of the tower width or the tower height.
c) For towers in staggered arrangement, the pedestrian exposure decreases with the building height heterogeneity (i.e., the roof height offset).
d) For staggered towers, the near-ground concentration decrease improves proportionally to the roof height offset. The highest decrease was found in the presence of three pieces of $T = 1.667H$ wide towers.
e) High-rise buildings can effectively mitigate pedestrian exposure to traffic-related air pollutants in matrix, intermediate, and staggered arrangements. The near-ground, as well as the canopy average concentration decrease is greater for three wide high-rise buildings ($T = 1.667H$) in a row compared to five slender ones ($T = H$).
f) Vertically elevating the buildings also results in a substantial concentration decrease, which grows with the ground clearance ($\Delta z/H = 0.1667\ldots 0.3333$).

Note that in cases a) – d), the plan area density of the buildings is kept constant ($\lambda_p = 0.5$). For the high-rise buildings (e), the plan area density is $\lambda_p = 0.25$, and for the elevated buildings (f) $\lambda_p = 0$.

The present study also highlights the importance of screening preliminary design ideas in the conceptual phase of the urban planning process. Following the parameter studies presented in this paper, potentially favorable building patterns were tested in detail via wind tunnel experiments and by CFD simulations in ANSYS Fluent [25], underlining the positive effect of roof height heterogeneity compared to uniform street canyons, as well as supporting the applicability of the presented GPU-based LES method for such investigations.

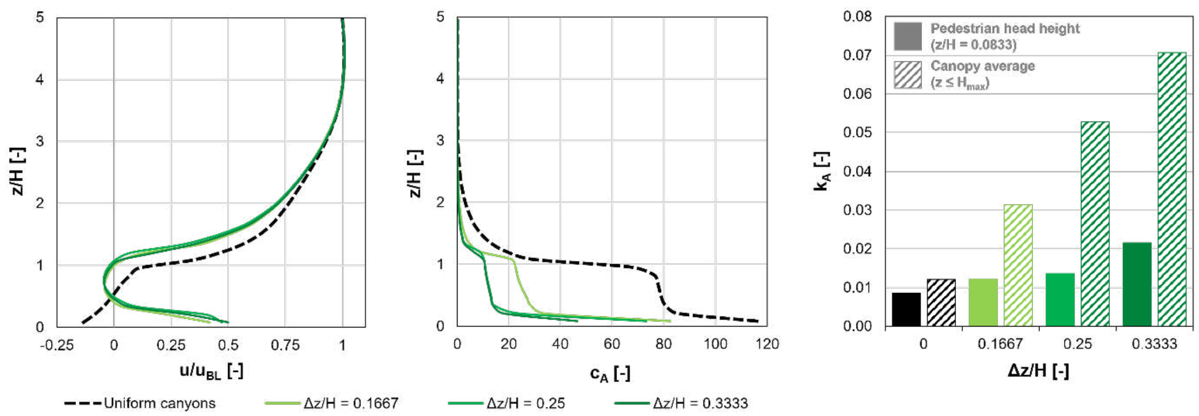

Figure 8. Elevated uniform buildings: the impact of the ground clearance (Δz), compared to the uniform canyons reference case (Δz = 0). The figure shows the vertical profiles of normalized velocity and concentration as well as the ventilation efficiency.

ACKNOWLEDGEMENTS

This study was funded by grant no. K 124439, NKFIH from the National Research, Development, and Innovation Office, Hungary. The research reported in this paper and carried out at BME has been supported by the NRDI Fund (TKP2020 NC, Grant No. BME-NCS) based on the charter of bolster issued by the NRDI Office under the auspices of the Ministry for Innovation and Technology. The research reported in this paper is part of project no. BME-NVA-02, implemented with the support provided by the Ministry of Innovation and Technology of Hungary from the National Research, Development and Innovation Fund, financed under the TKP2021 funding scheme. Bálint Papp's contribution to this paper was supported by the Gedeon Richter Talent Foundation (registered office: Gyömrői út 19-21, 1103 Budapest, Hungary), established by Gedeon Richter Plc., within the framework of the Gedeon Richter PhD Scholarship. The authors acknowledge the support of CFD.HU Ltd. in providing access to the necessary hardware and software, as well as express their gratitude towards Dipankar Choudhury (Vice President, Research) and Justin Hendrickson (Director of Product Management) of ANSYS, Inc. for providing insight to the simulation methods applied in ANSYS Discovery.

REFERENCES

[1] Tominaga, Y., & Stathopoulos, T. (2013). CFD simulation of near-field pollutant dispersion in the urban environment: A review of current modeling techniques. Atmospheric Environment, 79, 716-730. [DOI]

[2] Tominaga, Y., & Stathopoulos, T. (2016). Ten questions concerning modeling of near-field pollutant dispersion in the built environment. Building and Environment, 105, 390-402. [DOI]

[3] Blocken, B. (2018). LES over RANS in building simulation for outdoor and indoor applications: A foregone conclusion? Building Simulation, 11(5), 821-870). [DOI]

[4] da Silva, F. T., Reis Jr, N. C., Santos, J. M., Goulart, E. V., & de Alvarez, C. E. (2021). The impact of urban block typology on pollutant dispersion. Journal of Wind Engineering and Industrial Aerodynamics, 210, 104524. [DOI]

[5] Li, Z., Zhang, H., Wen, C. Y., Yang, A. S., & Juan, Y. H. (2020). Effects of height-asymmetric street canyon configurations on outdoor air temperature and air quality. Building and Environment, 183, 107195. [DOI]

[6] Du, Y., Mak, C. M., & Li, Y. (2018). Application of a multi-variable optimization method to determine lift-up design for optimum wind comfort. Building and Environment, 131, 242-254. [DOI]

[7] Hang, J., Li, Y., & Sandberg, M. (2011). Experimental and numerical studies of flows through and within high-rise building arrays and their link to ventilation strategy. Journal of Wind Engineering and Industrial Aerodynamics, 99(10), 1036-1055. [DOI]

[8] Hang, J., & Li, Y. (2012). Macroscopic simulations of turbulent flows through high-rise building arrays using a porous turbulence model. Building and Environment, 49, 41-54. [DOI]

[9] Chen, L., Hang, J., Sandberg, M., Claesson, L., Di Sabatino, S., & Wigo, H. (2017). The impacts of building height variations and building packing densities on flow adjustment and city breathability in idealized urban models. Building and Environment, 118, 344-361. [DOI]

[10] Huang, Y., Lei, C., Liu, C. H., Perez, P., Forehead, H., Kong, S., & Zhou, J. L. (2021). A review of strategies for mitigating roadside air pollution in urban street canyons. Environmental Pollution, 280, 116971. [DOI]

[11] Kluková, Z., Nosek, Š., Fuka, V., Jaňour, Z., Chaloupecká, H., & Ďoubalová, J. (2021). The combining effect of the roof shape, roof-height non-uniformity and source position on the pollutant transport between a street canyon and 3D urban array. Journal of Wind Engineering and Industrial Aerodynamics, 208, 104468. [DOI]

[12] Palusci, O., Monti, P., Cecere, C., Montazeri, H., & Blocken, B. (2022). Impact of morphological parameters on urban ventilation in compact cities: The case of the Tuscolano-Don Bosco district in Rome. Science of the Total Environment, 807, 150490. [DOI]

[13] Kristóf, G., & Füle, P. (2017). Optimization of urban building patterns for pollution removal efficiency by assuming periodic dispersion. Journal of Wind Engineering and Industrial Aerodynamics, 162, 85-95. [DOI]

[14] Kristóf, G., & Papp, B. (2018). Application of GPU-based Large Eddy Simulation in urban dispersion studies. Atmosphere, 9(11), 442. [DOI]

[15] Papp, B., Kristóf, G. (2019). Épületmintázatok optimalizálása a levegőminőség javításának érdekében GPU alapú nagyörvény szimulációval. XXVII. Nemzetközi Gépészeti Konferencia (OGÉT 2019) kiadványkötete (ISSN 2068-1267), 400-403.

[16] Szilágyi, M.Á., Papp, B. (2021). Miskolc átszellőzésének vizsgálata GPU-alapú nagyörvény szimulációval: XXVIIII. Nemzet-közi Gépészeti Konferencia (OGÉT 2021)

kiadványkötete (ISSN 2668-9685), 80-83. [PDF][Video]
[17] Papp, B., Kristóf, G., Gromke, C. (2020). Épületek szélterhelésének becslése GPU alapú nagyörvény szimulációval numerikus szélcsatornában: XXVIII. Nemzetközi Gépészeti Konferencia (OGÉT 2020) kiadványkötete (ISSN 2668-9685), 161-165. [PDF]
[18] Papp, B., Kristóf, G., & Gromke, C. (2021). Application and assessment of a GPU-based LES method for predicting dynamic wind loads on buildings. Journal of Wind Engineering and Industrial Aerodynamics, 217, 104739. [DOI]
[19] Smagorinsky, J. (1963). General circulation experiments with the primitive equations: I. The basic experiment. Monthly weather review, 91(3), 99-164. [DOI]
[20] Xie, Z., & Castro, I. P. (2006). LES and RANS for turbulent flow over arrays of wall-mounted obstacles. Flow, Turbulence and Combustion, 76(3), 291-312. [DOI]
[21] Courant, R., Friedrichs, K., & Lewy, H. (1967). On the partial difference equations of mathematical physics. IBM journal of Research and Development, 11(2), 215-234. [DOI]
[22] Snyder, W. H. (1981). Guideline for fluid modeling of atmospheric diffusion (Vol. 81, No. 9). Environmental Sciences Research Laboratory, Office of Research and Development, US Environmental Protection Agency. [PDF]
[23] Meroney, R. N. (2004). Wind tunnel and numerical simulation of pollution dispersion: a hybrid approach. Paper for Invited Lecture at the Croucher Advanced Study Institute, Hong Kong University of Science and Technology, 6-10. [PDF]
[24] Oke, T. R. (1988). Street design and urban canopy layer climate. Energy and buildings, 11(1-3), 103-113. [DOI]
[25] Papp, B., Kristóf, G., Istók, B., Koren, M., Balczó, M., & Balogh, M. (2021b). Measurement-driven Large Eddy Simulation of dispersion in street canyons of variable building height. Journal of Wind Engineering and Industrial Aerodynamics, 211, 104495. [DOI]

APPENDIX A1 – TYPICAL FLOW AND DISPERSION FIELDS

In this section, time-averaged velocity and normalized concentration distributions are presented in order to illustrate the flow and dispersion phenomena described in Section 3.

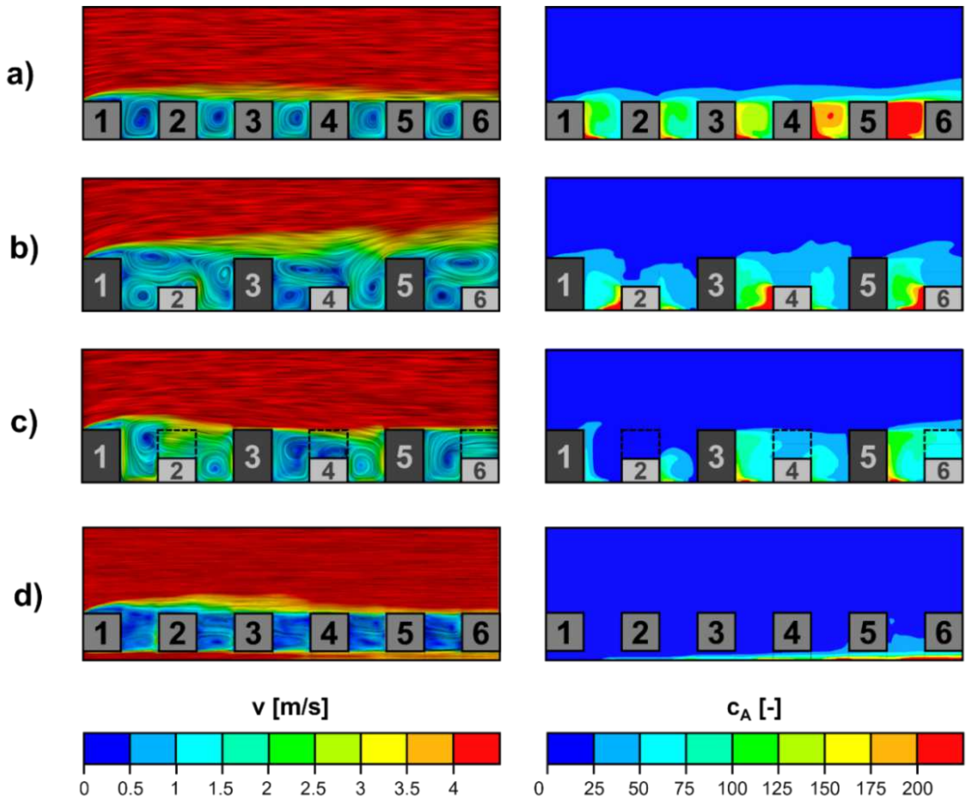

Figure A1. Flow and dispersion fields in the y/H = 0 vertical plane for building patterns of equal volume. a) uniform canyons; b) asymmetric canyons, $\Delta z/H$ = 0.375; c) towers on top of the buildings in staggered arrangement, $\Delta z/H$ = 0.375. d) elevated uniform buildings, $\Delta z/H$ = 0.25. Wind direction: from left to right.

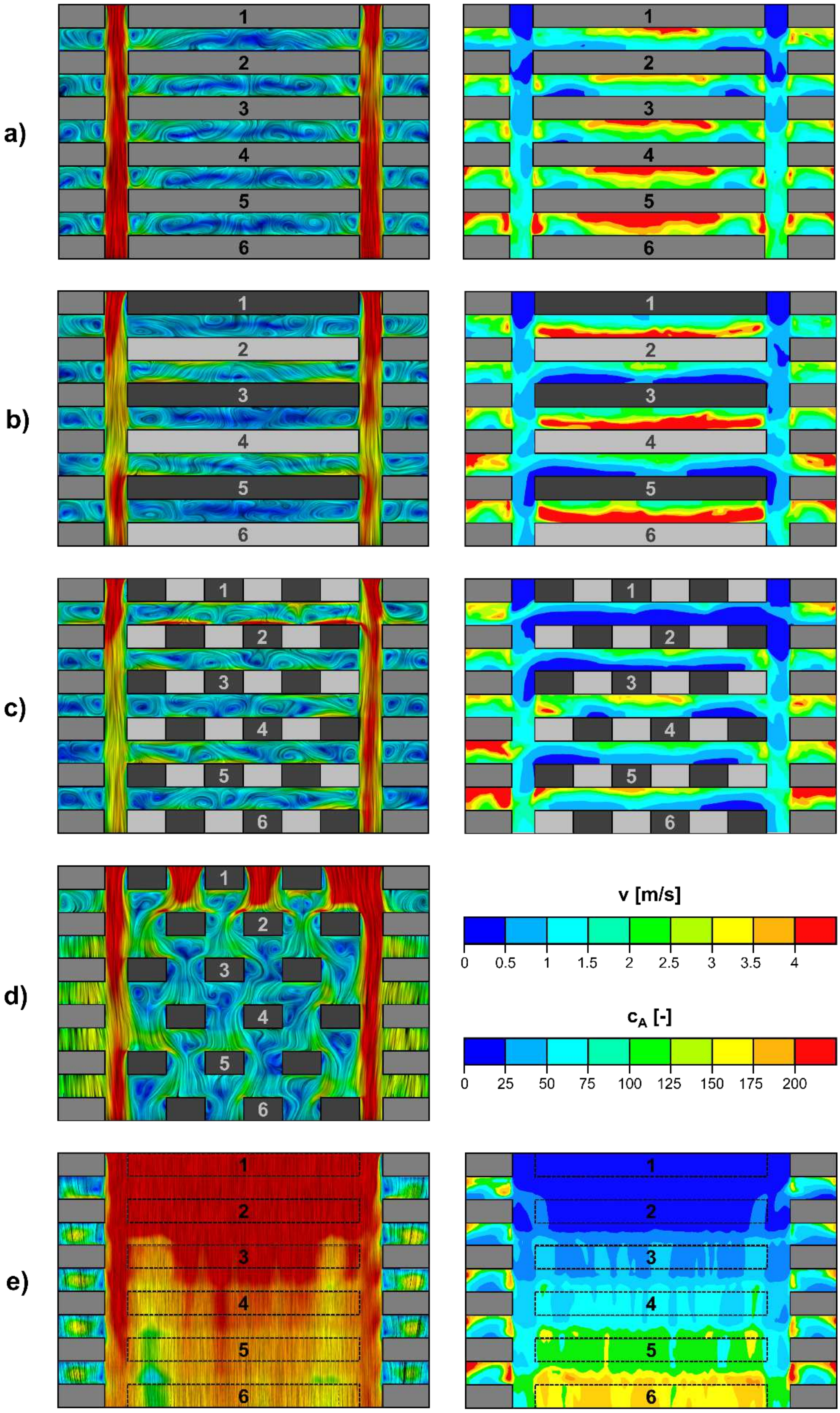

Figure A2. Flow and dispersion fields at pedestrian head height (in the $z/H = 0$ horizontal plane) for building patterns of equal volume. a) uniform canyons; b) asymmetric canyons, $\Delta z/H = 0.375$; c) three towers per row on top of the buildings in staggered arrangement, $\Delta z/H = 0.375$; d) flow field between the staggered towers at $z/H = 1.1875$; e) elevated uniform buildings, $\Delta z/H = 0.25$. Darker grey colors indicate taller buildings. Wind direction: from left to right.

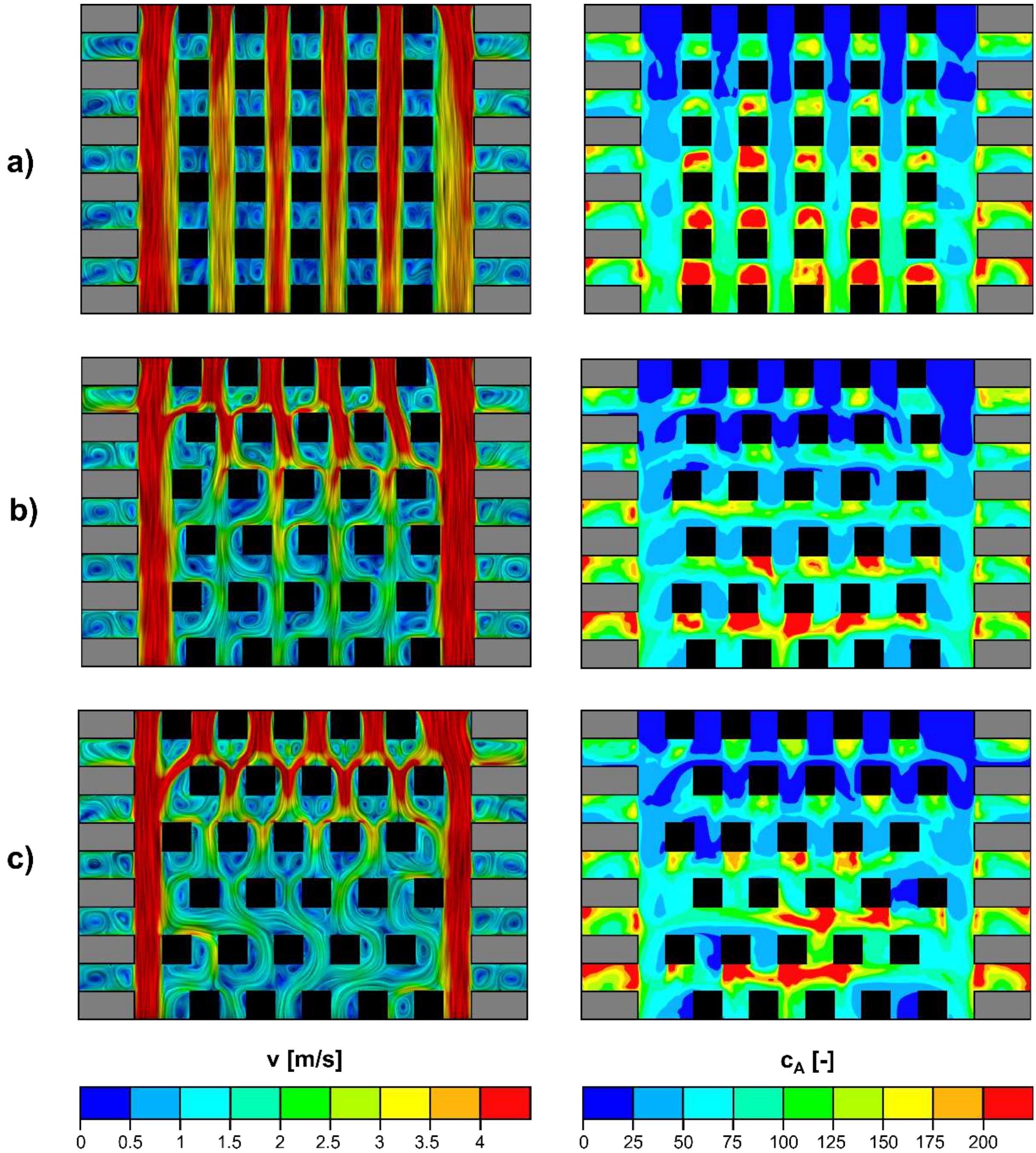

Figure A3. Flow and dispersion fields at pedestrian head height (*z/H* = 0.0833) for five, 2*H* tall high-rise buildings per row with different streamwise overlap of the buildings in consecutive rows. a) matrix arrangement, *Δy/T* = 1; b) intermediate arrangement, *Δy/T* = 0.5; c) staggered arrangement, *Δy/T* = 0. Wind direction: from top to bottom.

APPENDIX A2 – QUANTITATIVE RESULTS

Table A1. Summary of the analyzed building arrangements.

ID	Description	Geometrical parameters				Ventilation characteristics			Rank
		$\Delta z/H$ [–]	N [–]	T/H [–]	$\Delta y/T$ [–]	$c_{A,ng}$ [–] $c_{A,can}$ [–]	$\Delta c_{A,ng}$ [%] $\Delta c_{A,can}$ [%]	$k_{A,ng}$ [–] $k_{A,can}$ [–]	(1…28)
1	**Uniform street canyons** *Plan area density: $\lambda_p = 0.5$*	0	N.A.	N.A.	N.A.	116.1 82.6	N.A. N.A.	0.00861 0.01211	19 19
2	**Asymmetric street canyons** *Impact of the roof height heterogeneity* *Plan area density: $\lambda_p = 0.5$*	***0.25***	N.A.	N.A.	N.A.	123.0 69.8	+5.9 –15.4	0.00813 0.01432	28 29
3		***0.375***	N.A.	N.A.	N.A.	120.5 56.8	+3.7 –31.2	0.00830 0.01760	26 27
4		***0.5***	N.A.	N.A.	N.A.	78.3 40.9	–32.6 –50.4	0.01278 0.02442	11 19
5		***0.75***	N.A.	N.A.	N.A.	78.9 32.3	–32.1 –60.8	0.01268 0.03093	13 15
6	**Towers** *Impact of the tower width* ***Matrix (aligned) arrangement*** *Plan area density: $\lambda_p = 0.5$*	0.375	***2***	***2.5***	1	117.5 56.2	+1.2 –31.9	0.00851 0.01779	22 26
7		0.375	***3***	***1.667***	1	116.9 54.7	+0.6 –33.7	0.00856 0.01828	21 23
8		0.375	***4***	***1.25***	1	118.6 55.3	+2.1 –33.0	0.00843 0.01809	23 24
9		0.375	***5***	***1***	1	119.6 56.0	+3.0 –32.1	0.00836 0.01785	25 25
10	**Towers** *Impact of the tower width* ***Staggered arrangement*** *Plan area density: $\lambda_p = 0.5$*	0.375	***2***	***2.5***	0	71.5 35.3	–38.5 –57.3	0.01399 0.02837	8 16
11		0.375	***3***	***1.667***	0	67.7 35.4	–41.7 –57.2	0.01477 0.02827	7 17
12		0.375	***4***	***1.25***	0	77.0 40.8	–33.7 –50.6	0.01299 0.02450	10 18
13		0.375	***5***	***1***	0	79.7 42.5	–31.4 –48.5	0.01255 0.02350	16 20
14	**Towers** *Impact of the tower height* ***Matrix (aligned) arrangement*** *Plan area density: $\lambda_p = 0.5$*	***0.25***	3	1.667	1	116.1 64.7	0.00 –21.6	0.00861 0.01545	20 28
15		***0.5***	3	1.667	1	119.2 47.2	+2.6 –42.9	0.00839 0.02120	24 22
16		***0.75***	3	1.667	1	122.7 20.5	+5.6 –75.1	0.00815 0.04870	27 8
17 [1]		***1***	3	1.667	1	67.7 16.6	–41.7 –79.9	0.01477 0.06040	6 2
18	**Towers** *Impact of the tower height* ***Staggered arrangement*** *Plan area density: $\lambda_p = 0.5$*	***0.25***	3	1.667	0	79.1 46.0	–31.9 –44.3	0.01264 0.02173	15 21
19		***0.5***	3	1.667	0	64.1 30.2	–44.8 –63.5	0.01559 0.03315	4 13
20		***0.75***	3	1.667	0	65.6 24.8	–43.5 –70.0	0.01524 0.04037	5 9
21 [2]		***1***	3	1.667	0	62.4 18.2	–46.2 –78.0	0.01602 0.05496	3 4
22 [1]	**High-rise buildings** *Impact of the streamwise overlap* ***3 buildings*** *Plan area density: $\lambda_p = 0.25$*	1	3	1.667	***1***	67.7 16.6	–41.7 –79.9	0.01477 0.06040	6 2
23		1	3	1.667	***0.5***	51.9 19.9	–55.3 –75.9	0.01927 0.05027	2 6
24 [2]		1	3	1.667	***0***	62.4 26.0	–46.2 –68.5	0.01602 0.03841	3 10
25	**High-rise buildings** *Impact of the streamwise overlap* ***5 buildings*** *Plan area density: $\lambda_p = 0.25$*	1	5	1	***1***	87.3 20.3	–24.8 –75.4	0.01145 0.04918	18 7
26		1	5	1	***0.5***	78.5 26.6	–32.4 –67.8	0.01275 0.03764	12 11
27		1	5	1	***0***	79.1 28.0	–31.9 –66.1	0.01265 0.03574	14 12
28	**Elevated uniform buildings** *Impact of the ground clearance* *Plan area density: $\lambda_p = 0$*	***1.667***	N.A.	N.A.	N.A.	82.4 31.9	–29.0 –61.3	0.01213 0.03133	17 14
29		***0.25***	N.A.	N.A.	N.A.	73.2 19.0	–37.0 –77.0	0.01366 0.05272	9 5
30		***0.3333***	N.A.	N.A.	N.A.	46.4 14.1	–60.1 –82.9	0.02155 0.07071	1 1

[1,2] The marked cases are identical in terms of geometry and results. They are documented twice for a better understanding of the parameter studies. (Cases 17 and 22 as well as Cases 21 and 24.)

In Table A1 above, the following geometrical parameters and ventilation-related quantities are used:

H	[m]	reference building height
N	[–]	tower count or high-rise building count
T	[m]	tower width (in lateral direction)
Δy	[m]	streamwise overlap of the towers or high-rise buildings in consecutive rows
Δz	[m]	vertical offset of the roofs relative to the reference height H (+/– direction); or vertical offset of the entire building (i.e., ground clearance, + direction only)
λ_p	[–]	plan area density (the ratio of the total plan area of the buildings and the total ground area)
c_A	[–]	normalized concentration (the lower the better)
Δc_A	[%]	change in normalized concentration relative to the reference case (negative changes indicate air quality improvement)
k_A	[–]	mass Stanton number = dimensionless mass transfer coefficient = ventilation coefficient (the higher the better)

Subscripts and Superscripts:

ng	near-ground (average taken at pedestrian head height, $z/H = 0.0833$)
can	canopy average (average taken below roof height, $z \leq H_{max}$)